TELKOMNIKA Indonesian Journal of Electrical Engineering
Vol. 12, No. 10, October 2014, pp. 7287 ~ 7298
DOI: 10.11591/telkomnika.v12i8.5979

Land Surface Temperature Retrieval from the Medium Resolution Spectral Imager (MERSI) Thermal Data

Hailei Liu[1,2]*, Shenglan Zhang[1,2]
[1]College of Atmospheric Sounding, Chengdu University of Information Technology, Chengdu 610225, China;
[2]Institute of Atmospheric Physics, Chinese Academy of Sciences, Beijing 100029, China
*Corresponding author, e-mail: liuhailei@cuit.edu.cn

Abstract

A single channel land surface temperature (LST) retrieval algorithm named Single Channel Water Vapor Dependent (SCWVD) method was presented for Medium Resolution Spectral Imager (MERSI) thermal infrared band aboard FengYun-3A (FY-3A) satellite. Water Vapor Content (WVC) is the only input parameter in the algorithm assuming the surface emissivity is known. NCEP reanalysis monthly mean datasets are used to develop the SCWVD algorithm. Some tests, including global numerical simulations and validations with both in-situ measurements and MODIS LST product at Lake Tahoe, USA, were carried out to evaluate the algorithm performance. Compared with NCEP data and U.S. standard mid-latitude summer atmosphere model, the retrieved LST from simulated MERSI brightness temperature with MODTRAN had a RMSE about 0.8 K. In the validation, MERSI Level 2 water vapor product was employed, and the MERSI band emissivity was evaluated using the MODIS band 31 and 32 emissivity with an empirical expression. The results show that the difference between the retrieved MERSI LST and the in-situ measurements is less than 1 K in most situations. The comparison with the MODIS LST products (V5) shows that the RMSE is about 2.3 K.

Keywords: *MERSI, land surface temperature, water vapor content, single channel; band emissivity*

1. Introduction

Medium Resolution Spectral Imager (MERSI) is one of the 11 instruments aboard FY-3A spacecraft which is the first satellite of the second generation of Chinese polar-orbiting meteorological satellites launched on 27 May 2008. MERSI is a multispectral and medium-resolution spectral imager. It has 20 channels, of which there are four VIS and one TIR channels with a high spatial resolution of 250 m, which enables imaging of the Earth with high resolution in natural color during the day and high resolution TIR imaging during the night [1, 2]. These data improve our understandings of global dynamics and processes occurring on the land, oceans, and in the lower atmosphere. Details about some spectral properties of MERSI are listed in Table 1.

LST is a key parameter of the surface physical processes on regional and global scales. It plays an important role in many applications such as agriculture, geosciences, climate and other environmental studies [3-5]. Depending on the region where land surface processes are monitored, higher spatial and temporal resolutions are needed, which can be offered by FY-3A MERSI. However, like the Landsat missions, one of the main limitations of MERSI thermal information is the presence of only one channel in the TIR spectral region. It cannot use the split-window technique, the multi-channel method or the multi-angle method, which makes it more difficult to perform LST retrieval.

Several attempts have been done to perform LST retrieval for the Landsat 5 TM and Landsat 7 ETM+ TIR band [6-8], but few have been reported for MERSI data. What is more, most of those previous methods require information from atmospheric radiosoundings to perform atmospheric correction for LST retrieval. Qin et al. developed a mono-window LST retrieval algorithm for Landsat TM6 data using ground emissivity, atmospheric transmittance and effective mean atmospheric temperature as input parameters [9]. In the mono-window algorithm, the water vapor content (WVC) is designed as 0 to 3 g/cm^2, which limits LST retrieval

Received March 14, 2014; Revised July 14, 2014; Accepted August 3, 2014

when the actual WVC beyond 3g/cm^2. Moreover, air temperatures are not available when one wishes to retrieve LST over large areas. Jimënez-Muñoz and Sobrino developed a generalized single-channel method using WVC as the only input parameter, which minimizes the input data required and then provides an operational methodology to retrieve LST from the Landsat 5 thermal band [10, 11]. They used three parameters (Ψ1, Ψ2 and Ψ3) depending on WVC to retrieve LST. Each of the parameter has a relationship with WVC, which has been expressed by statistical fits. As three middle parameters (Ψ1, Ψ2 and Ψ3) have been used in the algorithm, more uncertainties would be introduced during fitting the middle parameter to WVC respectively. An error in the water vapor source could lead to another error in the three parameters, which will dramatically propagate to the LST retrievals. This problem is common to any technique based on a direct single-channel inversion of the radiation transferring equation (RTE), in which the final retrievals are very sensitive to uncertainties on the input parameters [12].

In this paper, an advanced operative single channel LST retrieval algorithm for MERSI TIR data was proposed. Assuming that land surface emissivity (LSE) is known, LST can be retrieved by this new advanced algorithm using WVC as the only input parameter. Compared with the previous methods, we mainly focused on improving the accuracy of retrieved LST by decreasing uncertainties introduced in the three parameters fitting to WVC, and the validity of this algorithm when the WVC in atmosphere beyond 3g/cm^2.

Table 1. MERSI Channel Characteristics (partial)

Channel	Wavelength(μm)	Bandwidth(μm)	Sub-point Resolution(m)	NEΔT / P (%) K (300K)	Primary use
3	0.650	0.05	250	0.4	Land surface emissivity
4	0.865	0.05	250	0.45	
5	11.25	2.5	250	0.5K	Land surface temperature
17	0.905	0.02	1000	0.10	
18	0.940	0.02	1000	0.10	Water vapor content
19	0.980	0.02	1000	0.10	

2. Theory and Methodology

2.1. Atmospheric Radiative Transfer

Generally speaking, the ground is not a blackbody, thus ground emissivity has to be considered for computing thermal radiance emitted by ground. Also atmosphere has important effects on the received radiance at remote sensor level. For a plane-parallel cloud free atmosphere under local thermodynamic equilibrium, ignoring scattering influence, the RTE describing the radiation intensity observed in channel *i* at zenith angle *θ*, can be formulated by including the radiance emitted by the ground, the upwelling radiation emitted by the atmosphere towards the sensor, and the downwelling radiation emitted by the atmosphere that reaches the Earth's surface and is then reflected towards the sensor. Therefore, the TOA radiance *Ii(θ)* measured by the satellite sensor in channel *i* at the zenith angle *θ* can be approximately expressed as [13]:

$$I_i(\theta)=B_i(T_i)=\tau_i(\theta)\varepsilon_i B_i(T_s)+I_i^{\uparrow}+\tau_i(\theta)(1-\varepsilon_i)I_i^{\downarrow} \quad (1)$$

Where T_s is the LST. $T_i(\theta)$, $\tau_i(\theta)$ and $\varepsilon_i(\theta)$ are the at-sensor brightness temperature, the atmospheric transmittance and ground emissivity in channel *i* at zenith *θ*. $I_i^{\uparrow}$ *and* $I_i^{\downarrow}$ is the atmospheric path and downward radiance, respectively. To obtain LST, three atmospheric parameters (τ, $I_i^{\uparrow}$ *and* $I_i^{\downarrow}$) and one band average emissivity should be determined.

In TIR band, the LST retrieval problem can be viewed as two interdependent processes: correction for the effects of the atmosphere, and the uncoupling of the surface temperature and emissivity. As for MERSI TIR data, the general objective of atmospheric correction algorithms is to remove the atmospheric effects, especially of water vapor absorption. And then an accurate estimation of the surface temperature and emissivity will be obtained.

2.2. The simplification of Planck's Function

In order to derive T_s from Equation (1), it is crucial to simplify the Planck's function especially for the single channel method and split-window algorithm [14, 15]. According to Qin [9], there is an approximate linearity between LST and Planck's radiance in 11.25μm. Therefore，the simplification of Planck's function can be expressed as follows:

$$B(T) = a + bT \quad (2)$$

Where a, b is the regression coefficients, and can be assigned -23.87, 0.1099 respectively with a RMSE of 0.06, When T is in the range of 260~300K.

2.3. The Derivation of Single Channel Algorithm for MERSI Data

The derivation of single channel algorithm is based on radiance transfer (1). According to the simplification of plank function mentioned above, the (1) can be rewritten as:

$$a + b*T_i = \varepsilon_i \tau_i(a+b*T_s) + I_i^{\uparrow} + \tau_i(\theta)(1-\varepsilon_i)I_i^{\downarrow} \quad (3)$$

Solving for Ts, we obtain the algorithm for LST retrieval from MERSI TIR data as follows:

Error! (4)

Equation (5) is rewritten in (6) for simplification：

$$T_s = ATi + B \quad (5)$$

Where, **Error!**, **Error!**.

Water vapor is the major absorber in the TIR, and WVC in the atmosphere varies both spatially and temporally, its effect on transmission in the TIR can also vary [16]. So it is important for the algorithm to use water vapor as an input variable to improve the accuracy of the LST retrieval [17]. As shown in Figure 1, coefficients (*A* and *B*) have a quadratic dependence on WVC (*w*) respectively. Thus, the relationship between coefficients (*A*, *B*) and WVC can be expressed as:

$$A = a1*w2 + a2*w + a3 \quad (6a)$$

$$B = b1*w2 + b2*w + b3 \quad (6b)$$

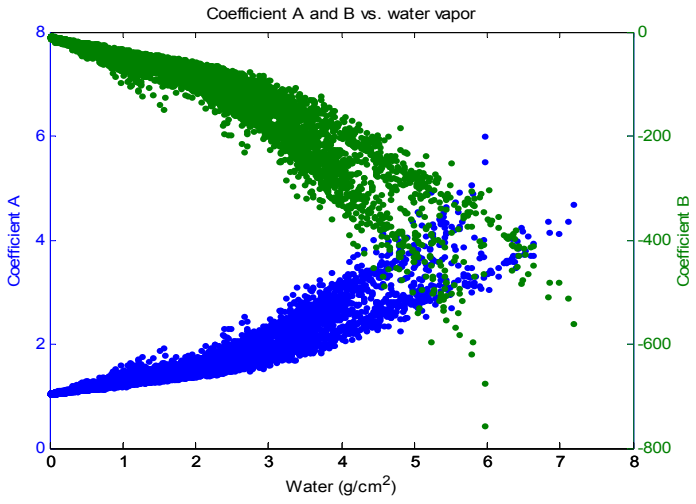

Figure 1. Relationship between the Two Coefficients (A, B) and WVC

Combining (6a) and (6b) with (5) results in a new relation to be derived between *Ts*, *Ti* and *w*:

$$T_s = (a1*w^2+a2*w+a3)Ti + b1*w^2+b2*w+b3 \quad (7)$$

Using a nonlinear regression technique, six coefficients a_i and b_i $(i=1,2,3)$ can be determined from (7). In the next section, we will address the progress for determination of the regression coefficients in details.

2.4. Determination of the SCWVD Coefficients

Global-based simulation datasets, including atmospheric profiles, surface temperature, and surface emissivity, were used to develop SCWVD algorithm.

The atmospheric profiles (geopotential height, air temperature, and humidity) were derived from monthly mean products (2.5 grid-point spacing) from NCEP climate data assimilation system (CDAS) reanalysis project [18]. We selected 467 pixels uniformly over land on global scales in January and July from 2000 to 2007 (see Figure 2(a)). Thus, there are 7472 samples in eight years. Then we carried out cloud detections over the 7472 samples using MODIS monthly fraction products [19] by setting a criterion as 0.3. If the cloud fraction in a pixel was larger than 0.3, it was considered as cloud contaminated, and the pixel was eliminated. At last, 6757 samples under cloud clear conditions were selected. As shown in Figure 2(b), 427 pixels were retained after cloud detection in January 2001.

In order to enlarge the validity of calculated coefficients, we did the following things: (1) LST was provided by adding -6, -3, 0, 3 and 6K to the surface air temperature of each profile. (2) LSE was set from 0.90 to 1.00 with 0.01 intervals increase. (3) The view zenith angle was set to be the values: 0°, 15° and 30°. (4) The surface elevation at each pixel was taken from USGS (U.S. Geological Survey) GTOPO30, and the satellite altitude is assumed to be 705 km. At last, 1,114,905 (6757×5×11×3) pairs of LST and the at-sensor brightness temperatures for the MERSI TIR bands are generated from the radiative transfer calculations (MODTRAN 4.0). The datasets were split into a training dataset used for calculating coefficients (780,434 patterns) and an independent test set used to evaluate its performance (334,471 patterns). The SCWVD coefficients were calculated by a least square method. Table 2 shows the derived coefficients. The RMSE for each SCWVD equation ranges from 0.81K to 0.91K at the different emissivity (0.90 to 1.00).

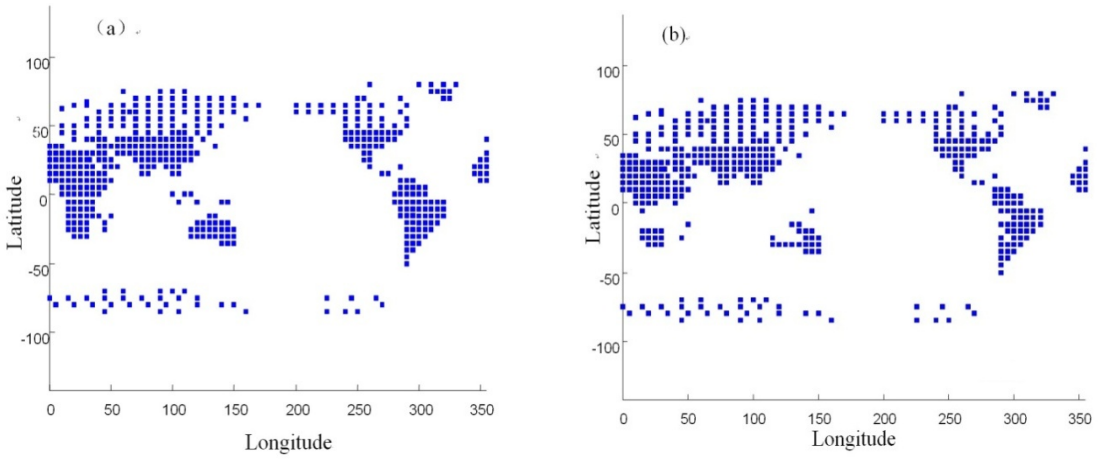

(a) (b)

Figure 2. (a) Global distribution of the 467 pixels; (b) Global distribution of retained 427 pixels after cloud detection in January 2001

Table 2. Coefficients and RMSE (in Kelvin) of Equation (7) for MERSI TIR Channel

Emissivity	a1	a2	a2	b1	b2	b3	RMSE (in K)
1.0000	0.014139	0.023359	1.0284	-4.1175	-5.4869	-5.4909	0.81
0.9900	0.015181	0.02238	1.0331	-4.4023	-5.3201	-6.1495	0.83
0.9800	0.016371	0.02088	1.0371	-4.7394	-4.9526	-6.6638	0.86
0.9700	0.016847	0.02063	1.0418	-4.8643	-4.9873	-7.3307	0.88
0.9600	0.016545	0.02212	1.0454	-4.788	-5.4445	-7.7097	0.89
0.9500	0.013779	0.02618	1.0497	-4.006	-6.6615	-8.2341	0.88
0.9400	0.012322	0.02883	1.0553	-3.5843	-7.5506	-9.0678	0.88
0.9300	0.008616	0.03033	1.0612	-2.5221	-8.1346	-9.9687	0.91
0.9200	0.002974	0.03149	1.0676	-0.88283	-8.7275	-10.964	0.87
0.9100	0.001608	0.02303	1.0742	-0.057323	-6.5891	-12.084	0.84

2.5. Sensitive Analysis

Provided that ground emissivity is known, the SCWVD algorithm for MERSI requires WVC as the only one parameter. Sensitivity and error analysis in term of the uncertainty of WVC in the atmosphere are presented in this section.

The sensitivity analysis of retrieved LST was carried out with the change of WVC in the standard atmosphere (Mid-latitude summer atmosphere, WVC = 2.92 g/cm2) simulated with MODTRAN 4.0. As shown in Figure 3, the LST error linearly increases with the WVC error rising in all cases, especially when the WVC is smaller than the truth value. When emissivity is low, the increasing of LST error is much slower. The maximum error does not exceed 0.8 K whatever the emissivity when the error on WVC is less than 0.5 g/cm2. In this case, the maximum error obtained depends more on the emissivity. If one considers only the cases emissivity larger than 0.95, the maximum error on the retrieved temperature does not exceed 0.6 K when the error on W is less than 0.5 g/cm2. As a conclusion, the sensitivity of the SCWVD method to errors on SCWVD increases for greater WVC and lower emissivity.

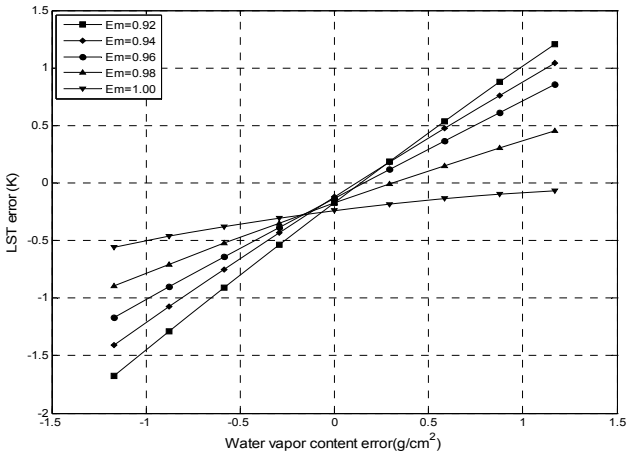

Figure 3. Relationships between the retrieved LST error and WVC error at given different emissivity

2.6. Land Surface Emissivity and Water Vapor Content

2.6.1. Land Surface Emissivity

It is very challenging to accurately estimate land surface emissivity (LSE) at the global scale. For water surface which is comparatively homogeneous, a constant emissivity can be assumed; for land surface, the LSE dynamics have wider range and can vary over short distance. Several methods have been reported on the basis of either the normalized difference vegetation index (NDVI) or the land cover information [20-24]. Red and NIR channels of MERSI in Table 1 can be used to derive NDVI for calculating LSE.

In this research, an empirical expression was built to evaluate the MERSI band emissivity using the MODIS band 31 and 32 emissivity. Figure 4(a) gives MERSI and MODIS

thermal infrared band spectral responses function. MERSI thermal band is located in the region 8~14μm [25, 26]. It is possible to estimate the MERSI band emissivity using MODIS band 31 and 32 emissivity due to the lower emissivity values variation in 8-14μm. In order to analyze the relationship between the MERSI and MODIS thermal infrared band emissivity. Surface emissivity was provided by using 55 materials (water, snow/ice, vegetation, and soil, etc.) selected from a spectral library (http://speclib.jpl.nasa.gov/) [27]. Then, the band average emissivity was calculated using the selected JPL emissivity spectra convolved with the MERSI and MODIS response function. Figure 4(b) shows the relationship between MERSI thermal band emissivity and the average emissivity of MODIS band 31 and band 32. The final expression for MERSI LSE is given by: εmersi=0.791(εmodis31+εmodis32)+0.204. In our validation, we will use the MODIS Land emissivity product (MOD11_L2) to derive MERSI emissivity maps for the LST retrieval.

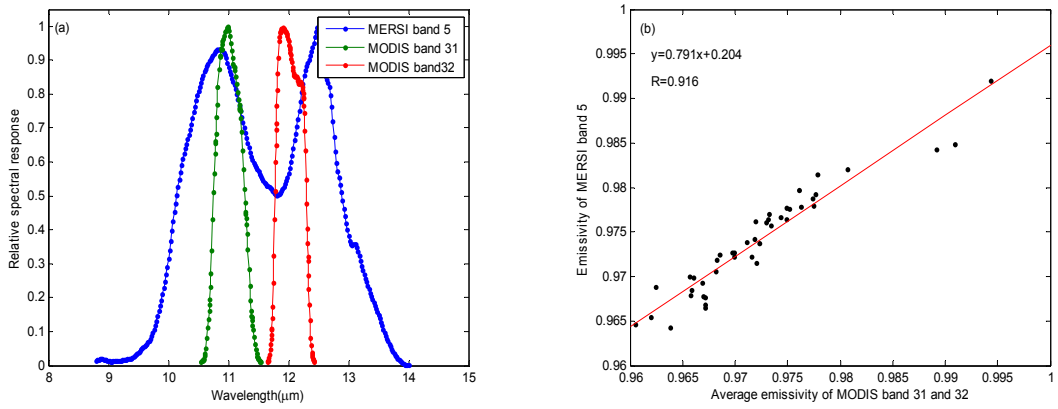

Figure 4. (a) Thermal band response functions for MERSI and MODIS; (b) Relationship between MERSI Thermal band emissivity and the average emissivity of MODIS band 31 and band 32

2.6.2. Water Vapor Content

As shown in Table 1, MERSI has three channels which can be used to estimate WVC, including strong water vapor absorption line at 0.940μm, weak water vapor absorption line at 0.905μm and atmospheric window at 0.980μm. The WVC can be derived using the reflected solar radiance measurement [28, 29]. In this research, the MERSI L2 PWV product is used. The details of the MERSI L2 PWV algorithm can be found in [30]. The method adopted here for PWV retrieval is based on the ratio of reflected solar radiance detected by satellite between water vapor absorption channels and atmospheric window channels. By employing channel ratios, the aerosol extinction distribution and the variation effect of surface reflectance are partially removed, and the atmospheric transmittance of water vapor channels is approximately obtained. The PWV is derived from the atmospheric transmittance based on a Look up Table which is pre-calculated using a radiation transfer model. The sensitivities of atmospheric transmission in each NIR water vapor channels of MERSI to the total perceptible water vapor are also simulated. The result indicates that FY-3A/MERSI has and good ability in detecting NIR water vapor, and can demonstrate fine characteristic of PWV spatial distributions with 20% relative error to the sounding. They have assessed the PWV L2 WVC accuracy, the retrieved WVC from MERSI NIR are compared with the ground based sounding data. Over cloud free area, there is a good agreement between them in variation trend and spatial distribution.

3. Results and Discussion

3.1. Numerical Tests of the Algorithm

3.1.1. Standard atmosphere Simulation Results

In this section, we apply the SCWVD algorithm to retrieve LST to evaluate its performance. The best way to validate an algorithm is to compare the in-situ ground truth

measurements of LST with the retrieved one. However, this is not feasible, for it is extremely difficult to obtain the in-situ ground truth measurements which must be comparable to the pixel size of MERSI data at the satellite pass. A practical way is to use the simulated data generated by atmospheric simulation programs such as LOWTRAN, MODTRAN or RTTOV [31].

The simulation with the mid-latitude summer atmosphere was carried out to test our algorithm. MODTRAN 4.0 was used in the calculation. Detailed results are listed in Table 3, when the WVC in mid-latitude summer atmosphere is 2.92 g/cm2. The results indicate the algorithm is able to provide a quite accurate estimation of LST, with the difference between the assumed LST and the retrieved less than 0.5 K in most cases. It is encouraging that the result is good at several different emissivity.

Table 3. Validation of SCWVD Algorithm for the Mid-latitude Summer Atmosphere

Emissivity	R	Tb	Ts_truth	Ts_truth-Tb	LSTSCWVD	Ts_truth- LSTSCWVD (Error)
1.00	7.865503	288.4949	295.00	6.5051	294.5252	0.4748
0.98	7.771243	287.7112	295.00	7.2888	294.5644	0.4356
0.96	7.676987	286.9221	295.00	8.0779	294.5562	0.4438
0.94	7.582730	286.1276	295.00	8.8724	294.5204	0.4796
0.92	7.488467	285.3274	295.00	9.6726	294.3825	0.6175

3.1.2. NCEP/CDAS Reanalysis Simulation Results

Global-based simulation datasets as mentioned in section 2.4 were used to test SCWVD algorithm. Figure 5(a) depicts the difference between LST retrieved using the SCWVD method and LST get from global assimilation data. Figure 5(b) represents the relations between the errors of retrieved LST using the SCWVD method and WVC. As shown in Figure 5(b), the absolute errors of retrieved LST in global area are mainly concentrated in the range of±1.5K, with a RMSE of 0.87K. We also found that the retrieval errors are mainly located in the range of ±1K, when WVC is less than 1.5g/cm2. However, When WVC is larger than 3g/cm2, the retrieval errors can reach up to 2K.

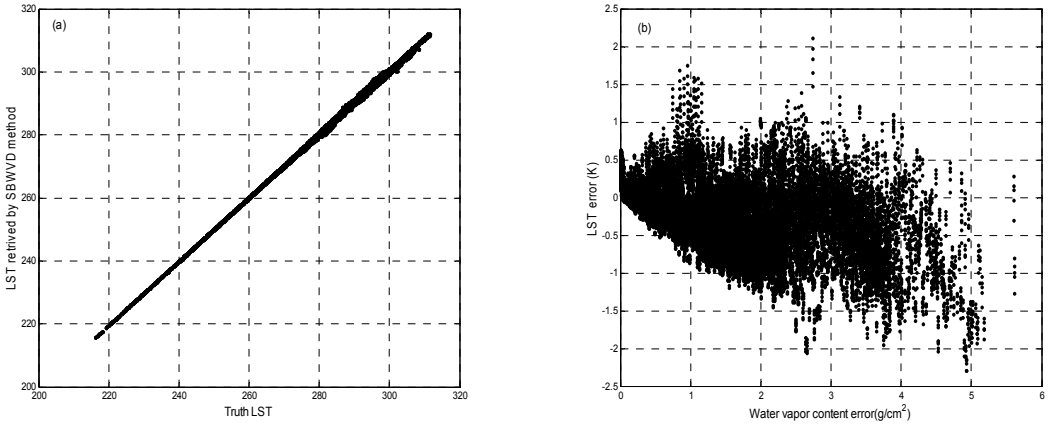

Figure 5. (a) Relationship between the truth LST (NCEP) and the retrieved LST by SCWVD method. (b) Relationship between LST error and WVC

3.2. Tests Using In-situ Measurements in Lake Tahoe and MODIS Product

The objective of the present work is to estimate the LST from the second generation of China's polar-orbiting meteorological satellite FY-3A MERSI observation over the cloud-free area. The TOA brightness temperatures are directly extracted from the MERSI L1B satellite data. The LSE map was derived from the MODIS LSE product according to the method motioned above. The WVC are obtained from MERSI L2 total perceptible water product, which can be accessed from FENGYUN Satellite Data Center (http://fy3.satellite.cma.gov.cn/). FY-3A

MERSI Level 2 water vapor product is used as the input parameter for the SCWVD method, and a 2-D data interpolation procedure is applied in order to match the MERSI L1B data in spatial resolution.

In order to validate our presented algorithm, the Lake Tahoe, CA/NV, USA, is selected as the study area. NASA scientists selected Lake Tahoe as a validation site just before the Terra satellite was launched in 1999 on a 15-year mission to study Earth's environment [32]. Equipped with a suite of instruments that constantly monitor the lake environment, the rafts and buoys provide information that helps make sure that Earth-observing satellites are getting their temperature measurements right. Measurements at the site are made from four permanently moored buoys on the lake, referred to as TB1, TB2, TB3, and TB4. Each buoy has a custom-built radiometer that measures the skin temperature and several temperature sensors that measure the bulk water temperature. The automated validation site, where ground measurements of lake skin temperature have been made on a near continuous basis (every 2 min) since 1999 and used to calibrate and validate TIR data and products from airborne and satellite instruments, including the ASTER, MODIS, Landsat 5 TM, the Landsat 7 TM and ATSR [32-37]. Figure 6 gives the current location of the measurement sites on a map.

As SCWVD algorithm is developed for cloud clear conditions, cloud detection should be done first. In this section, the SCWVD method is validated using MERSI scenes acquired around Lake Tahoe in 2009. Twelve MERSI and MODIS scenes were selected from June to October. Table 4 gives the Data acquisition details of the various daytime MERSI and MODIS scenes. The difference of MERSI and MODIS overpass time was within 30 minutes in most cases. Taking into account the lake surface is relatively uniform, LST changes caused by the time difference is negligible. The MODIS LST products have been validated within 1K in multiple validation sites in relatively wide ranges of surface and atmospheric conditions. We tested SCWVD algorithm g in more than 10 clear-sky cases according to compare the MERSI retrieved LST with in-situ measurement data and MODIS LST product.

Table 4. Data Acquisition Details of Various Daytime Imagery of MERSI and MODIS

Date	Julian Day	MERSI overpass time	MODIS overpass time
2009.6.9	160	18:30	19:00
2009.6.16	167	19:10	18:55
2009.6.18	169	18:30	19:00
2009.7.2	183	19:10	19:00
2009.7.4	185	18:30	18:55
2009.8.3	215	19:10	18:55
2009.8.5	217	18:30	18:55
2009.8.28	240	18:00	18:55
2009.9.13	256	18:30	19:00
2009.9.29	272	19:35	18:55
2009.10.9	282	18:10	19:30
2009.10.22	295	19:05	19:00

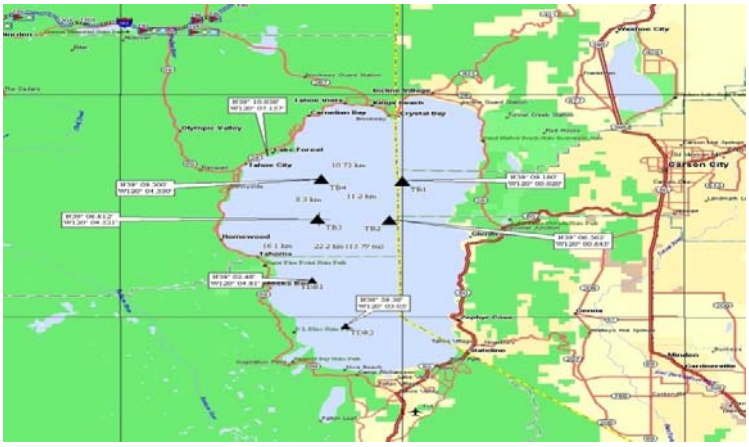

Figure 6. Current Location of the Measurement Sites on the Map (from http://laketahoe.jpl.nasa.gov)

The difference of MERSI and MODIS overpass time was within 30 minutes in most cases. Taking into account the lake surface is relatively uniform, LST changes caused by the time difference is negligible. The MODIS LST products have been validated within 1K in multiple validation sites in relatively wide ranges of surface and atmospheric conditions. We tested SCWVD algorithm g in more than 10 clear-sky cases according to compare the MERSI retrieved LST with in-situ measurement data and MODIS LST product.

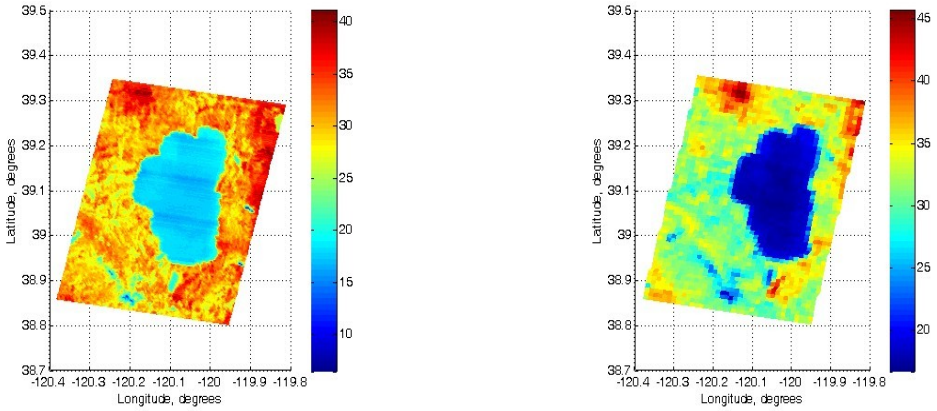

(a) (b)

Figure 7. (a) Retrieved LST using SCWVD algorithm from MERSI L1B data over Lake Tahoe at 03h UTC, 3 Aug. 2009; (b) MODIS LST product over Lake Tahoe at same time

Figure 7(a) depicts the surface temperature distribution retrieved by SCWVD method for MERSI scene acquired around 03h UTC on 3 August 2009. Figure 7(b) give the MODIS LST product (provided by NASA) around Lake Tahoe. Obviously, the surface temperatures in Qinghai Lake range in 16~18℃ and the temperature distribution is quite uniform with the average value of 16.7K which is near the value measured by the buoy (17.5◦C). The LST around the Lake Tahoe is obviously higher than water face with the average value about 30℃. Taking into account the spatial-resolution difference between MERSI and MODIS, match-up was generated employing the 2-D interpolation. Figure 8(a) gives the error distribution map between MERSI LST with MODIS LST product. For the water surface temperature, the maximum difference is about 1.2 K, most of the differences are around 0.5 K, and the RMSE is 0.35 K. The largest temperature difference was obtained outside lake with an error of 4.7 K. We think the main reason maybe the effect of spatial-resolution difference and the implement of the interpolation. Figure 8(b) gives the scattering plot of the retrieved MERSI LST and MODIS LST product with an RMSE of 2.3K. The results indicate that most of the retrieved LSTs from MERSI data are a little higher than that from MODIS LST products around the lake. It is worth noticing that MERSI LST has great improvement than MODIS in the spatial resolution, for example, MERSI can easily get the temperature changes information of the small water body nearby the Lake Tahoe.

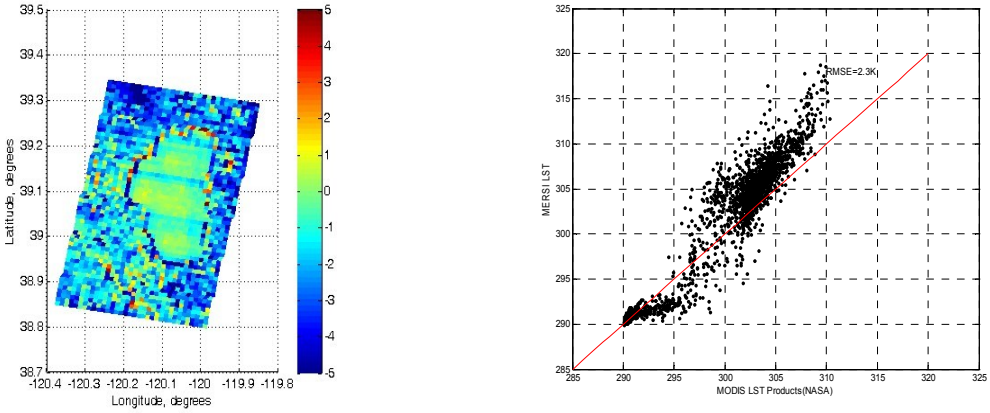

Figure 8. (a) Difference between MERSI LST with MODIS LST product (provided by NASA); (b) Comparison between the derived MERSI LST and MODIS LST

The LSTs retrieved by the SCWVD algorithm have also been compared with in-situ measurements in Lake Tahoe. Figure 9 give the difference between MERSI, MODIS and buoy measurement water surface skin temperature over the 12 days (4 buoys measurements average per day). The results indicate that the accuracy of the retrieved MERSI LSTs is less than 1.5K. The MODIS LST accuracy is better than MERSI's.

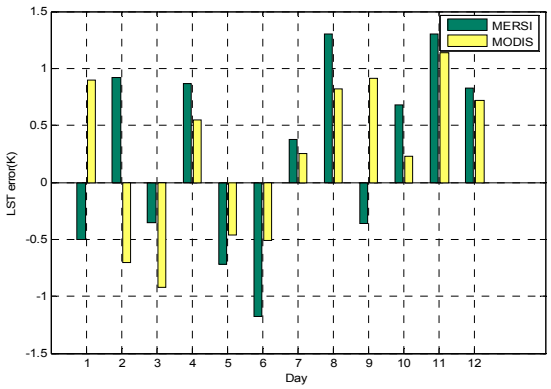

Figure 9. Comparison of the LST Error between the MERSI, MODIS LSTs and In-situ Measured LSTs in Lake Tahoe

4. Conclusion

As a new generation of polar orbiting meteorological satellite, FY-3 series consists of two experimental and at least four operational satellites, which is expected to have a service life until 2020. Launched respectively on 27 May 2008 and 5 November 2011, FY-3A and FY-3B are designed with the same assignments and equipped with 11 payloads. The only difference is that FY-3A is a morning-observation satellite and FY-3B is an afternoon-observation satellite. These two satellites can provide global observation of the Earth Land surface temperature with high spatial resolution (250m) four times per day, which is a great improvement comparison to the current LST products of other satellite in the temporal and spatial.

Based on the upper background, we developed a SCWVD algorithm for LST retrieval from MERSI TIR data. The derivation of this algorithm is based on the thermal radiance transfer equation and the linearization of Planck's radiance function. Totally there are two critical parameters in the algorithm: emissivity and WVC. On giving those two parameters, it will be very easy to use this algorithm for LST estimation not only from MERSI data but also from

others. Moreover, the approach does not need radiosonde data or local meteorological observations. The principle of algorithm can be also extended to other sensors having one or more TIR channels such as TM and ETM+ aboard Landsat series satellite.

Tests with the simulated datasets suggest that the SCWVD algorithm has a high accuracy for LST retrieval. Compared with NCEP data and U.S. standard mid-latitude summer atmosphere model, the retrieved LST from simulated MERSI brightness temperature with MODTRAN had a RMSE about 0.8 K. Further application of the SCWVD algorithm is carried out at Lake Tahoe. The result shows that the difference between the retrieved MERSI LST and the LST measured by the buoy is less than 1.5K. Comparison between LST retrieved by SCWVD algorithm and MODIS LST product suggests that the SCWVD algorithm is applicable and feasible in actual conditions, with the RMSE about 2.3 K. It should be pointed out that the LST estimated from the MERSI measurement has not been validated with in-situ measurements over land pixels. In the future, we will validate the SCWVD algorithm over land and compare the retrieved LST from MERSI TIR data with the well validated MODIS LST product.

Acknowledgements

This work is supported by National Satellite Meteorological Center, CMA by Grant FY3-PGS-0603 and the Tibet Meteorological Administration & CUIT S&T Cooperation Project. The authors would like to thank Dr. Zhang Yong and Dr. Zhang Liyang for their valuable comments and suggestions.

References

[1] Dong CH, Yang J, Zhang WJ, Yang ZD, Lu NM, Shi JM, Zhang P, Liu YJ, Cai B. An overview of a new Chinese weather satellite fy-3a. *B Am Meteorol Soc*. 2009; 90: 1531.
[2] Hu XQ, Sun L, Liu JJ, Ding L, Wang XH, Li Y, Zhang Y, Xu N, Chen L. Calibration for the solar reflective bands of medium resolution spectral imager onboard fy-3a. *IEEE T Geosci Remote.* 2012; 50: 4915-4928.
[3] Wan ZM, Dozier J. Land-surface temperature-measurement from space - physical principles and inverse modeling. *IEEE T Geosci Remote*. 1989; 27: 268-278.
[4] Wan ZM, Dozier J. A generalized split-window algorithm for retrieving land-surface temperature from space. *IEEE T Geosci Remote*. 1996; 34: 892-905.
[5] Yu Y, Privette JL, Pinheiro AC.,, Evaluation of split-window land surface temperature algorithms for generating climate data records. *IEEE T Geosci Remote.* 2008; 46: 179-192.
[6] Yang Y, Yan DM. *An improved algorithm for land surface temperature retrieval from landsat-5 thermal infrared data in tianjin binhai new area.* Proc Spie 2010; 7831.
[7] Li FQ, Jackson TJ, Kustas WP, Schmugge TJ, French AN,Cosh MH, Bindlish R. Deriving land surface temperature from landsat 5 and 7 during smex02/smacex. *Remote Sens Environ*. 2004; 92: 521-534.
[8] Jimenez-Munoz JC, Cristobal J, Sobrino JA, Soria G, Ninyerola M, Pons X. Revision of the single-channel algorithm for land surface temperature retrieval from landsat thermal-infrared data. *IEEE T Geosci Remote*. 2009; 47: 339-349.
[9] Qin Z, Karnieli A, Berliner P. A mono-window algorithm for retrieving land surface temperature from landsat tm data and its application to the israel-egypt border region. *Int J Remote Sens*. 2001; 22: 3719-3746.
[10] Sobrino JA, Jimenez-Munoz JC,Paolini L. Land surface temperature retrieval from landsat tm 5. *Remote Sens Environ*. 2004; 90: 434-440.
[11] Jimenez-Munoz JC, Sobrino JA. A generalized single-channel method for retrieving land surface temperature from remote sensing data. *J Geophys Res-Atmos*. 2003; 108.
[12] Cristobal J, Jimenez-Munoz JC, Sobrino JA, Ninyerola M, Pons X. Improvements in land surface temperature retrieval from the landsat series thermal band using water vapor and air temperature. *J Geophys Res-Atmos*. 2009; 114.
[13] Becker F, Li ZL. Towards a local split window method over land surfaces. *Int J Remote Sens.* 1990; 11; 369-393.
[14] Franca GB.; Cracknell AP. Retrieval of land and sea-surface temperature using NOAA-11 avhrr data in north-eASTERn brazil. *Int J Remote Sens*. 1994; 15: 1695-1712.
[15] Coll C, Caselles V, Sobrin JA, Valor E. On the atmospheric dependence of the split-window equation for land-surface temperature. *Int J Remote Sens*. 1994; 15: 105-122.
[16] SteynRoss ML, Steyn Ross DA. *Land surface temperature retrieval from avhrr: Influence of surface emissivity and atmospheric water vapor.* Igarss '96 - 1996 International Geoscience and Remote Sensing Symposium: Remote Sensing for a Sustainable Future. 1996; I - Iv : 2098-2100.

[17] Francois C, Ottle C. Atmospheric corrections in the thermal infrared: Global and water vapor dependent split-window algorithms - applications to ATSR and avhrr data. *IEEE T Geosci Remote*. 1996; 34: 457-470.
[18] Kalnay E, Kanamitsu M, Kistler R, Collins W, Deaven D, Gandin L, Iredell M, Saha S,White G, Woollen J. et al. The ncep/ncar 40-year reanalysis project. *B Am Meteorol Soc*. 1996; 77: 437-471.
[19] Platnick S., Wind G, King MD, Holz RE, Ackerman SA, Nagle FW. *Comparison of the modis collection 5 multilayer cloud detection product with calipso.* Aip Conf Proc. 2009; 1100: 416-419.
[20] Becker F. The impact of spectral emissivity on the measurement of land surface-temperature from a satellite. *Int J Remote Sens*. 1987; 8: 1509-1522.
[21] Valor E, Caselles V. Mapping land surface emissivity from ndvi: Application to european, african, and south american areas. *Remote Sens Environ*. 1996; 57: 167-184.
[22] Li ZL, Becker F. Feasibility of land surface-temperature and emissivity determination from avhrr data. *Remote Sens Environ.* 1993; 43: 67-85.
[23] Snyder WC, Wan Z, Zhang Y, Feng YZ. Classification-based emissivity for land surface temperature measurement from space. *Int J Remote Sens.* 1998; 19: 2753-2774.
[24] Sobrino JA, Jimenez-Munoz JC, Soria G, Romaguera M, Guanter L, Moreno J, Plaza A, Martincz P. Land surface emissivity retrieval from different vnir and tir sensors. *IEEE T Geosci Remote.* 2008; 46: 316-327.
[25] Schmugge T, Hook SJ, Coll C. Recovering surface temperature and emissivity from thermal infrared multispectral data. *Remote Sens Environ*. 1998; 65: 121-131.
[26] Gillespie A.; Rokugawa S.; Matsunaga T.; Cothern J.S.; Hook S.; Kahle AB. A temperature and emissivity separation algorithm for advanced spaceborne thermal emission and reflection radiometer (ASTER) images. *IEEE T Geosci Remote*. 1998; 36: 1113-1126.
[27] Baldridge AM.; Hook SJ.; Grove CI.; Rivera G. The ASTER spectral library version 2.0. *Remote Sens Environ*. 2009; 113: 711-715.
[28] Gao BC, Kaufman YJ. Remote sensing of water vapor and thin cirrus clouds using modis near-ir channels. *Optical Remote Sensing of the Atmosphere and Clouds Ii*. 2001; 4150: 217-224.
[29] Kaufman YJ, Gao BC. Remote-sensing of water-vapor in the near ir from eos/modis. *IEEE T Geosci Remote*. 1992; 30: 871-884.
[30] Hu Xiuqing, Huang Yibin, Lu Qifeng, Zheng Jing. Retrieving Precipitable Water Vapor Based on the Near infrared Data of FY 3A Satellite. *Journal of Applied Meterological Science*. 2011; 22(1): 46~56.
[31] Dash P, Gottsche FM, Olesen FS, Fischer H. Land surface temperature and emissivity estimation from passive sensor data: Theory and practice-current trends. *Int J Remote Sens.* 2002; 23: 2563-2594.
[32] Hook SJ, Prata FJ, Alley RE, Abtahi A, Richards RC, Schladow SG, Palmarsson SO. Retrieval of lake bulk and skin temperatures using along-track scanning radiometer (ATSR-2) data: A case study using lake tahoe, california. *J Atmos Ocean Tech*. 2003; 20: 534-548.
[33] Ellicott E, Vermote E, Petitcolin F, Hook SJ. Validation of a new parametric model for atmospheric correction of thermal infrared data. *IEEE T Geosci Remote*. 2009; 47: 295-311.
[34] Hook SJ, Clodius WB, Balick L, Alley RE, Abtahi A, Richards RC, Schladow SG. In-flight validation of mid- and thermal infrared data from the multispectral thermal imager (mti) using an automated high-altitude validation site at lake tahoe ca/nv, USA. *IEEE T Geosci Remote*. 2005; 43: 1991-1999.
[35] Hook SJ, Vaughan RG, Tonooka H, Schladow SG. Absolute radiometric in-flight validation of mid infrared and thermal infrared data from ASTER and modis on the terra spacecraft using the lake tahoe, ca/nv, USA, automated validation site. *IEEE T Geosci Remote*. 2007; 45: 1798-1807.
[36] Hulley GC, Hook SJ. Intercomparison of versions 4, 4.1 and 5 of the modis land surface temperature and emissivity products and validation with laboratory measurements of sand samples from the namib desert, namibia. *Remote Sens Environ*. 2009; 113: 1313-1318.
[37] Thome K, Arai K, Hook S, Kieffer H, Lang H, Matsunaga T, Ono A, Palluconi F, Sakuma H, Slater P, et al. ASTER preflight and inflight calibration and the validation of level 2 products. *IEEE T Geosci Remote.* 1998; 36; 1161-1172.